NAVAL POSTGRADUATE SCHOOL
Monterey, California

THESIS

EXPERIMENTAL DAMAGE STUDIES
FOR A
FREE ELECTRON LASER WEAPON

by

Robert W. Thomson Jr.

June 1999

Thesis Advisor:	William B. Colson
Second Reader:	Robert L. Armstead

Approved for public release; distribution is unlimited.

19990818 281

REPORT DOCUMENTATION PAGE

1. AGENCY USE ONLY *(Leave blank)*	2. REPORT DATE June 1999	3. REPORT TYPE AND DATES COVERED Master's Thesis

4. TITLE AND SUBTITLE EXPERIMENTAL DAMAGE STUDIES FOR A FREE ELECTRON LASER WEAPON	5. FUNDING NUMBERS
6. AUTHOR(S) Thomson, Robert W., Jr.	

7. PERFORMING ORGANIZATION NAME(S) AND ADDRESS(ES) Naval Postgraduate School Monterey, CA 93943-5000	8. PERFORMING ORGANIZATION REPORT NUMBER

9. SPONSORING / MONITORING AGENCY NAME(S) AND ADDRESS(ES)	10. SPONSORING / MONITORING AGENCY REPORT NUMBER

11. SUPPLEMENTARY NOTES

The views expressed in this thesis are those of the author and do not reflect the official policy or position of the Department of Defense or the U.S. Government.

12a. DISTRIBUTION / AVAILABILITY STATEMENT Approved for public release; distribution is unlimited.	12b. DISTRIBUTION CODE

13. ABSTRACT *(maximum 200 words)*

Laser material damage experiments for this thesis were the first ever conducted at the new DoE Thomas Jefferson National Accelerator Facility (TJNAF) free electron laser (FEL) user laboratory. In the past only large-scale laser experiments were thought to properly model weapons applications. Experimental procedures developed in this thesis allowed a scaled-down laser of a few hundred Watts to characterize the damage from a weapon-scale one million Watt laser. The TJNAF FEL has the power of a microwave oven concentrated into a beam the size of a pencil lead. The unique TJNAF FEL beam bombards the target with a steady stream of tens of millions of pulses per second each containing 50 million Watts of power in a short burst of 4×10^{-13} seconds. No other laser combines these characteristics, and no experiments have previously been done to explore the effects of the FEL pulse. Target materials were obtained from the Naval Research Laboratory (NRL) and from Naval Surface Warfare Division (NSWD) Port Hueneme. Data were collected and analyzed using video cameras, optical microscopes and a scanning electron microscope (SEM). This thesis has been a productive cooperation among NPS, TJNAF, NRL, and NSWD Port Hueneme, to the benefit of DoD.

14. SUBJECT TERMS Free Electron Laser, Directed Energy Weapons, Laser Damage Experiments	15. NUMBER OF PAGES 59
	16. PRICE CODE

17. SECURITY CLASSIFICATION OF REPORT Unclassified	18. SECURITY CLASSIFICATION OF THIS PAGE Unclassified	19. SECURITY CLASSIFI- CATION OF ABSTRACT Unclassified	20. LIMITATION OF ABSTRACT UL

i

EXPERIMENTAL DAMAGE STUDIES FOR A FREE ELECTRON LASER WEAPON

Robert W. Thomson Jr.
Lieutenant Commander, United States Navy
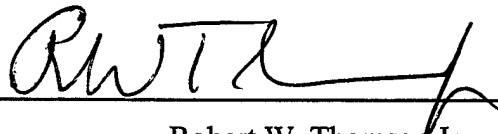B.S.E, University of Pennsylvania, 1987

Submitted in partial fulfillment of the
requirements for the degree of

MASTER OF SCIENCE IN APPLIED PHYSICS
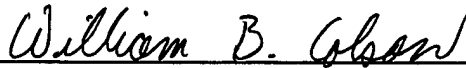
from the

NAVAL POSTGRADUATE SCHOOL
June 1999

Author: _____
Robert W. Thomson Jr.

Approved by: _____
William B. Colson, Thesis Advisor

_____
Robert L. Armstead, Second Reader

_____
William Maier, Chairman
Department of Physics

ABSTRACT

Laser material damage experiments for this thesis were the first ever conducted at the new DoE Thomas Jefferson National Accelerator Facility (TJNAF) free electron laser (FEL) user laboratory. In the past only large-scale laser experiments were thought to properly model weapons applications. Experimental procedures developed in this thesis allowed a scaled-down laser of a few hundred Watts to characterize the damage from a weapon-scale one million Watt laser. The TJNAF FEL has the power of a microwave oven concentrated into a beam the size of a pencil lead. The unique TJNAF FEL beam bombards the target with a steady stream of tens of millions of pulses per second each containing 50 million Watts of power in a short burst of 4×10^{-13} seconds. No other laser combines these characteristics, and no experiments have previously been done to explore the effects of the FEL pulse. Target materials were obtained from the Naval Research Laboratory (NRL) and from Naval Surface Warfare Division (NSWD) Port Hueneme. Data were collected and analyzed using video cameras, optical microscopes and a scanning electron microscope (SEM). This thesis has been a productive cooperation among NPS, TJNAF, NRL, and NSWD Port Hueneme, to the benefit of DoD.

TABLE OF CONTENTS

I. INTRODUCTION

This thesis argues that the Navy has a need for new weapons to provide ship self-defense against sea-skimming missiles in littoral waters. Since the Navy's Directed Energy Office has already selected the free electron laser (FEL) for developmental funding, this thesis describes the FEL as a candidate weapon. The primary thrust of the thesis is to describe laser damage experiments conducted at the Thomas Jefferson National Accelerator Facility (TJNAF). These are the first experimental tests that study the damage from a short pulsed laser at a high repetition rate with a few hundred Watts of average power. The unique idea advanced in this thesis is that scaling rules can be developed that will allow these small-scale damage experiments to represent the damage from a large, MW-scale weapon.

A.   SHORTCOMINGS OF CURRENT SHIP SELF-DEFENSE SYSTEMS

With the collapse of the Soviet Union and the fading from memory of the cold war era bipolar world, a "new world order" was supposed to have emerged. There were rosy predictions of a world without conflict where the nations of the earth coexisted in peace and prosperity. Now less than ten years after the fall of the Berlin Wall, we see that those predictions were grossly optimistic, and that new challenges have arisen for the art of diplomacy and for military science. We have had constant bloodshed from the Gulf War to the never-ending ethnic violence in the Balkans. In addition, many countries whose interests do not coincide with the interests of the United States seem to be vigorously pursuing programs to develop weapons of mass destruction and advanced

missile technology. Many of these countries' programs seem to have been enhanced by the break-up of the Soviet Union, which has made weapons technology and technicians available to the highest bidder.

The U.S. military by contrast has been obliged to "do more with less" due to budget cuts, while changing weapons procurement and tactics to meet emerging threats. For the U.S. Navy, there is no longer another navy in the world to pose a threat on the high seas, and the primary focus has shifted to the littoral with emphasis on power projection ashore from the sea and support of land forces. This new operating environment has revealed vulnerabilities of U.S. Naval forces. These vulnerabilities were not anticipated when current ship's systems were being designed and built during the cold war's uncertain aftermath. The primary vulnerability of U.S. Navy ships is attack by high-speed anti-ship missiles and is exacerbated by operating in the littoral environment.

1. Surface-To-Air-Missiles (SAMs)

The first line-of-defense for most ships is the Standard Missile, which is launched vertically and designed to destroy incoming missiles at long range. These systems, along with ships' long-range radars, are ideally suited to the open ocean environment with visibility limited only by the curvature of the earth. In the littoral on the other hand, conditions are often quite different. Because ships often operate within a few miles of land, the detection range for incoming missiles is severely curtailed with subsequent drop in reaction time. Due to the speed of modern anti-ship missiles, and the short ranges of the littoral, the Detect-To-Engage (DTE) sequence for the Standard Missile will be impossible to execute in the time available.

Furthermore, these Standard Missile systems are not installed on all Navy ships, but only on the cruisers and the destroyers, about two-thirds of the ships. The rest of the ships have no "long range" anti-ship missile defense at all, for either the open ocean or the littoral. The system is very expensive both in terms of money and in terms of the space required. Since a ship has a very limited budget of space, and the missile magazine, the missile launching system, and associated radars are large and heavy, it is impractical to ever put them on logistics ships or amphibious ships. Cruisers and destroyers will have enough problems defending themselves from missile attack in the littoral, and will therefore be completely incapable of defending other ships.

2. Close-In-Weapon-System (CIWS)

All ships that might operate in the littoral do have the CIWS, which is a short-range gun and radar system designed to destroy an inbound missile just before it gets to the ship. CIWS has never been tested in battle conditions. Computer simulations indicate that it is unlikely the system can destroy an anti-ship missile at ranges greater than 100-200 meters. Although the gun has a nominal range of 2000 meters, penetrator dispersion seriously degrades the effective range of the system. CIWS has an average dispersion of two to three milliradians or 0.17 degrees, which leads to a probability of a bullet hitting the target as shown in Figure (1). The system has a probability of hitting the target of very nearly 0% from its maximum range all the way in to about 500 meters. The probability does not rise above 10% until the inbound missile is within 200 meters of the ship. As the missile approaches the ship the probability of a hit increases and the accumulated hits can be calculated by applying the appropriate probabilities for each 100-meter increment of the missiles path.

Single Round Intercept Probability
CIWS Height 25m, Dispersion 3mrads, Missile Height 5m
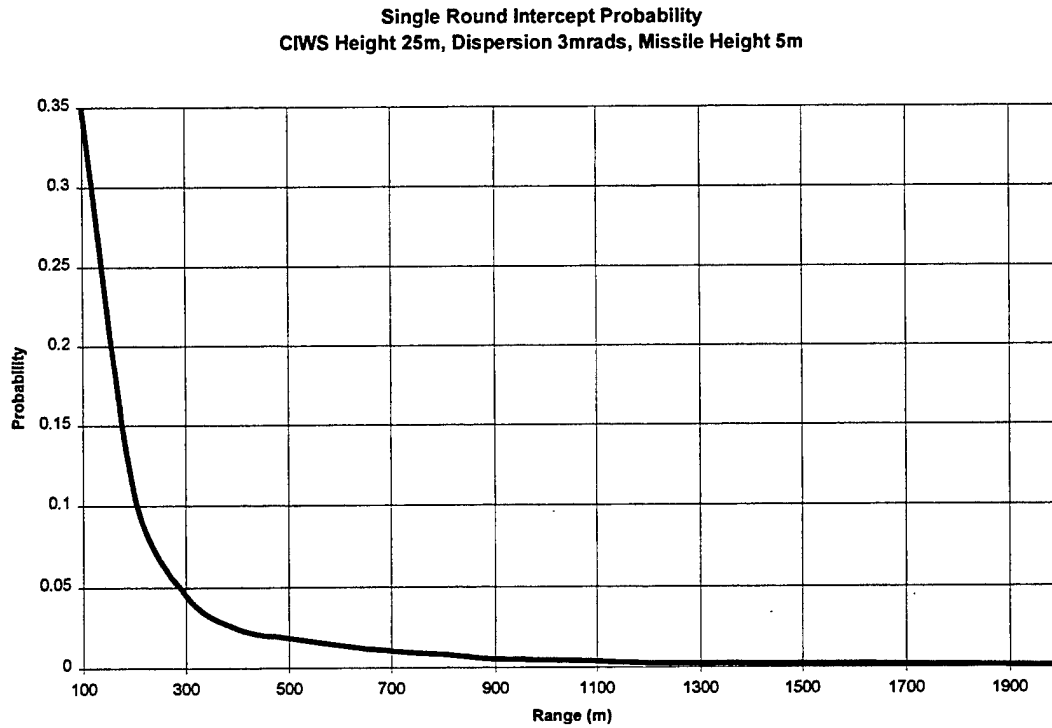
Figure 1. Single Round Intercept Probability

Assuming a relatively slow, non-maneuvering missile, and assuming it takes an average of eight hits to kill a missile, Figure (2) shows that the kill range will be 100-200 meters as mentioned above. Killing the missile with multiple hits is not the end of the story. Once the missile breaks up, the fragments can still hit the ship and cause damage. The computer simulation was extended to analyze the trajectories of post-kill missile fragments.
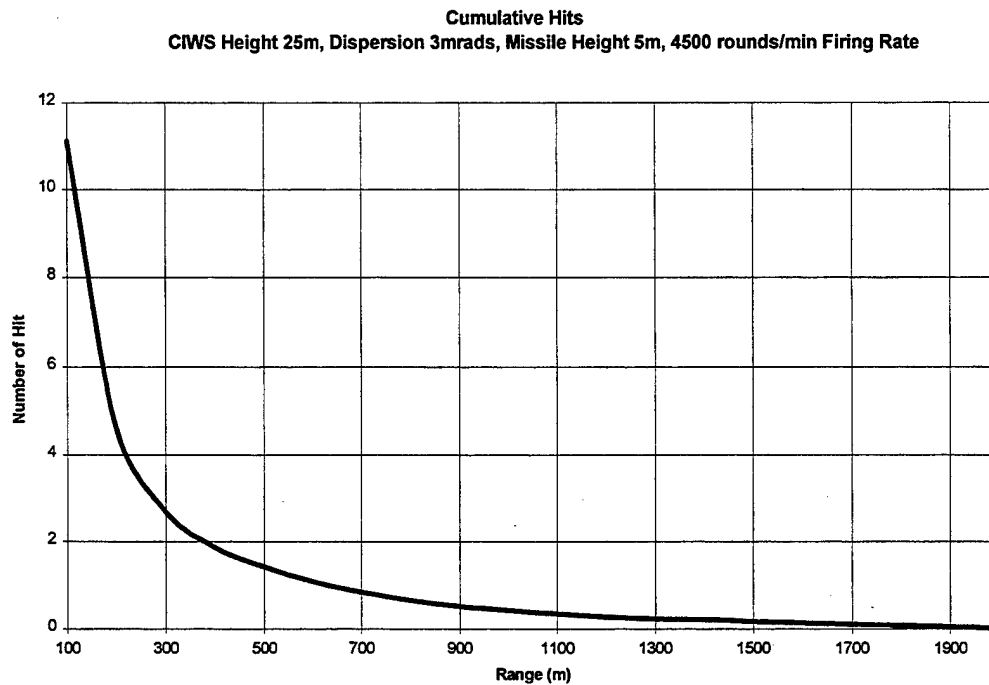
Figure 2. Cumulative Hits vs. Range

The shorter the kill range, the more likely that many missile fragments will strike the ship. Figure (3) shows this to be the case, and in fact at the likely kill range for CIWS, about 50% of the missile fragments will hit the ship with the average fragment having a mass of 40Kilograms, a velocity of 50 meters/second and kinetic energy of 50000 Joules. If the missile could be destroyed at 1000 meters or greater from the ship the probability of damage from missile fragments would be small. CIWS, however, is not capable of killing targets at those ranges.

Probability of a Fragment Striking the Ship
Missile Speed 600m/s, Missile Height 5m, 10000 Fragments Sampled Every 100m
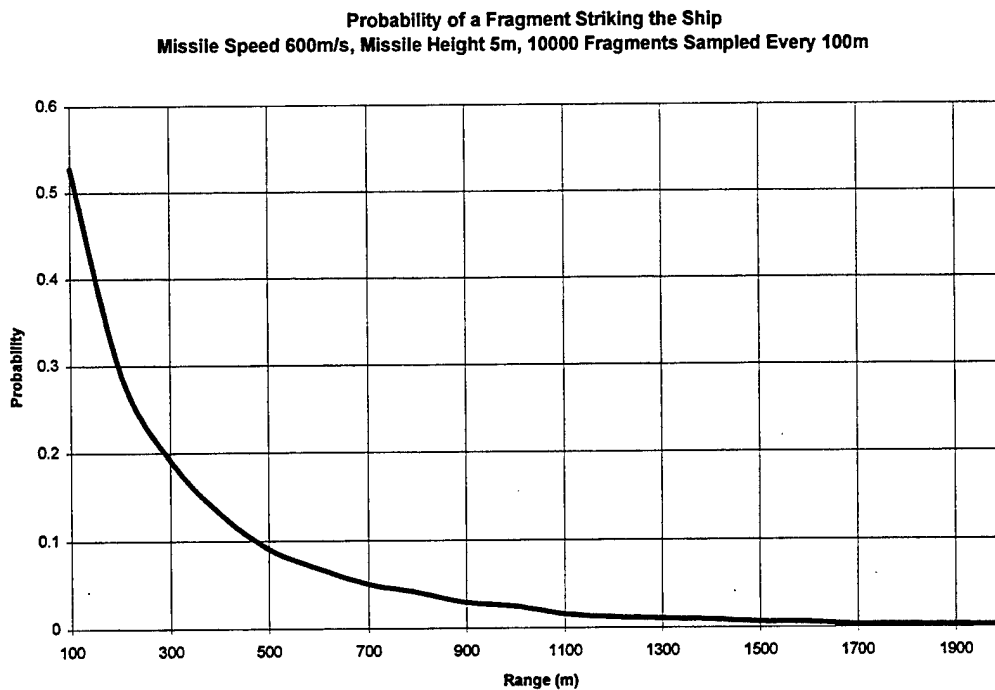
Figure 3. Probability of Fragment Striking Ship vs. Kill Range

So even under ideal conditions for CIWS with ample warning to commence

engagement at maximum range, a slow, non-maneuvering missile leaves the phalanx

system inadequate for ship self-defense. Under more realistic littoral conditions with little

or no advance warning of an attack, and a fast, maneuvering missile the CIWS will be

nearly useless. A new ship self-defense system is required.

B.   DIRECTED ENERGY WEAPONS

One promising possibility is to use beams of high energy focused on an incoming

missile to destroy it at long range. A major advantage of this type of weapon is that it

travels at 300 million meters per second. Since the missile can only travel at a few

hundred meters per second, any maneuver the missile makes becomes meaningless. There are three major methods of generating the large energies necessary to destroy an anti-ship missile in flight: Particle Beams, High Powered Microwaves (HPM), and Lasers. All of these technologies have been studied for many decades to determine their suitability as anti-missile weapons. The advantages and disadvantages of each will be discussed in turn to see where the scientific research has lead so far.

1.   Particle Beams

The idea of using a high-energy beam of subatomic particles, electrons, protons or neutrons, to shoot down a missile has been around since the early 1970's, but was given major consideration and funding as part of the Strategic Defense Initiative (SDI) in the 1980's. Of all the possible Directed Energy Weapons the Particle Beam seems to face the most serious obstacles.

The main problem for an electron beam anti-missile weapon is propagation loss, which has three major components: Ionization Loss, Bremstrahlung Loss, and Beam Divergence due to elastic scattering. Ionization Loss occurs when energy from the beam ionizes surrounding air molecules and amounts to approximately 0.34 MeV/m. This means that a 500 MeV electron beam would travel less than 1500 meters even if there were no other loss mechanism. But there are other loss mechanisms. Bremstrahlung Loss is caused when beam electrons are accelerated in curved paths around atomic nuclei due to coulomb interaction. The electron beam then loses energy by emitting Bremstrahlung photons. Bremstrahlung Loss alone would limit a 500 MeV beam to a propagation path of about 360 meters. Elastic scattering of the beam occurs when electrons "collide" with more massive air molecules as in Bremstrahlung Loss and the trajectories of the electrons

are changed. This causes the electron beam to spread as it propagates through the air. Elastic scattering alone would cause a 500 MeV electron beam to dissipate in 240 meters [Ref. 1]. Actual experimentation with all loss mechanisms working together shows that an electron beam only propagates a few meters through the air.

2. High Powered Microwaves (HPM)

HPM technology seems to hold more promise than particle beams because of the maturity of the field and we know we can propagate them through the air. But HPM weapons also face challenges. Assuming that an adequate source of HPM is available there are generally two methods of employment to defeat incoming missiles. One is to aim an intense beam at a specific target to destroy it at long range, and the other is to sweep a large area in the hope of disabling many targets. The second method is unattractive for military applications because of the lower probability of kill for each target and because of the increased likelihood of fratricide.

Once a source is found and a tactic is chosen, the HPM radiation must reach the target by propagation through the atmosphere. Atmospheric attenuation of HPM at sea is dominated by suspended particles such as dust and water droplets, which condense during rain or fog. Figure (4) shows that in the absence of fog or rain, a water vapor absorption peak at 22 GHz and an oxygen absorption peak at 60 GHz dominate attenuation of HPM. There is a relative minimum in attenuation at 35 GHz. Once the radiation reaches the target there are two basic transmission paths into the electronics of the missile. The "front-door" path is one designed to transmit microwaves in the normal operation of the system, and the "back-door" path is one of radiation coupling through a path not designed for transmission. It requires less energy on target to defeat a missile by

8

the front-door path, but there is certainly no guarantee that the enemy will cooperate and
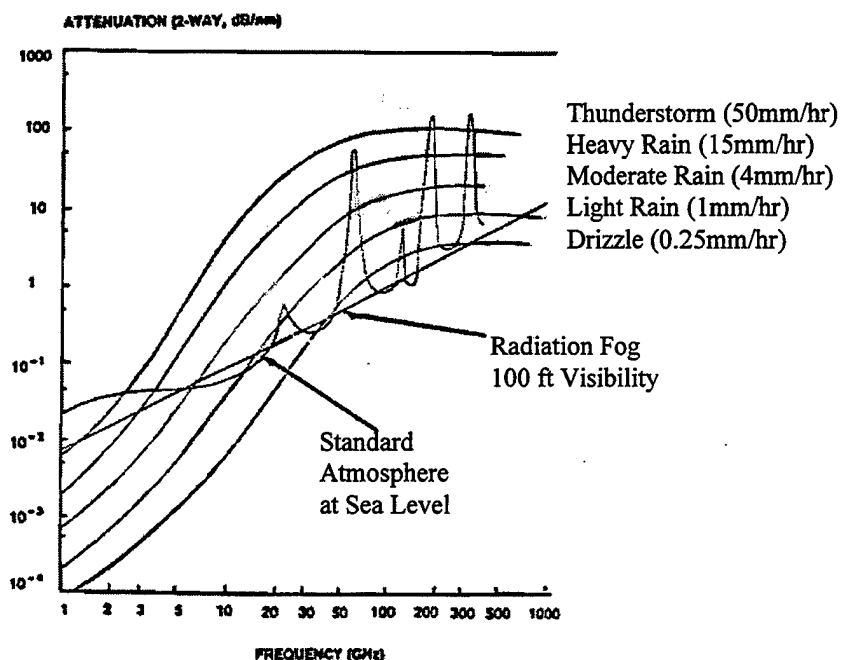
design missiles appropriately.

ATTENUATION (2-WAY, dB/nm)

Figure 4. Atmospheric Attenuation of HPM, From Ref. [2]

An additional problem for HPM weapons is the ease of shielding against them.

Herbert, using a digital watch and a microwave oven, conducted simple experiments that

were quite enlightening. A three-second exposure to microwaves caused an unshielded

watch to quit working. When a similar watch was placed in a box made of aluminum foil

and placed in the microwave, it was able to withstand repeated exposure including

individual exposures of as long as 90 seconds with no loss of function [Ref 3]. Assuming

a relatively slow missile capable of 300 m/s, the shielded missile would travel 27

Kilometers during that 90 seconds and the ship would be dead.

Another problem for long wavelength HPM is diffraction. Beam spread angle is proportional to wavelength by the relation $\theta = 1.22\,\lambda\,/\,D$, where D is the aperture size. Beam spot area is then $A = \pi\,(R\theta)^2$, where R is the range to the target. With an antenna diameter of 10 meters and a wavelength of 6 cm (5 GHz), the beam spot is 4208 m^2 at a range of 5 km. The energy is spread over a wide area and the effectiveness of the weapon reduced.

3.   Lasers

Lasers are in use in our society today for so many mundane purposes that we take them for granted. We use them as pointers for presentations in offices, to play our music and movies at home, to cut things in industry, and to perform surgery in hospitals. Laser weapons have excited the American imagination for decades. In the 1950's early science fiction shows had "ray guns", in the 1960's *Star Trek* had "phasors", in the 1970's and 1980's *Star Wars* had "Death Stars" with lasers which could destroy entire planets at a shot. The scientific community has worked hard in conjunction with the military to explore the potential of the laser as a weapon. The first proof of this potential was the Air Force's ALL project in the 1970's, followed by the Navy's MIRACL project in the 1980's, and the Air Force's ABL program in the 1990's [Ref. 4]. There are many different types of lasers that have different strengths and weaknesses, and all must be judged against the stringent requirements of a shipboard laser weapon.

The laser must be able to emit enormous power, but be small enough to fit on a ship. It must operate at a wavelength that propagates well through the atmosphere, so that range does not suffer. It must not produce dangerous byproducts that cannot be disposed

of at sea. We shall look more closely at each one of these criteria and see how the available lasers stack up.

4.   **Atmospheric Propagation**

It is important to study the transmission of laser radiation through the atmosphere, because certain wavelengths, and therefore certain lasers, can be eliminated on the basis that they cannot propagate 5 km to the target with sufficient energy to destroy a target. A non-linear phenomenon known as thermal blooming can occur with high power lasers when the air is stagnant and the target is approaching on a constant bearing. The air between the ship and the target is heated, changing the index of refraction, and forming an effective lens that can disperse the laser beam. Since thermal blooming is a non-linear effect, the more power in the beam, the faster thermal blooming will occur. As a result it is critical to find a wavelength with the minimum absorption and, therefore, maximum transmission through the atmosphere. Figure (5) shows atmospheric transmittance for wavelengths of interest for lasers, but the finer detail is necessary to pick an exact window for optimal transmission. There are regions of high transmittance in the 3-5 micron band and the 8-12 micron band, which have been the typical wavelengths for IR sensors. There are much smaller sections of the spectrum, which give close to 100% transmittance at 1.042 μm, 1.06 μm, 1.6 μm, 2.2 μm, and 3.8μm. Cook and Albertine have done a more detailed study of this issue in relation to a maritime deployed high-energy laser weapon system (HELWS). Their conclusions are summarized in Figures (6) and (7), which show the most promising wavelength to minimize absorption and the thermal blooming problem is 1.042 μm.
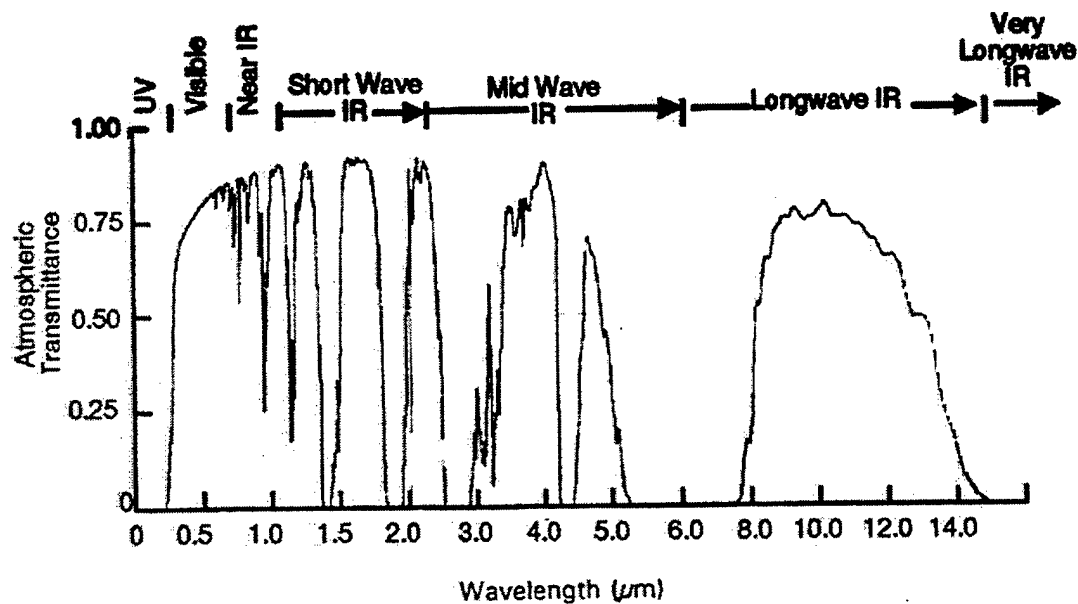
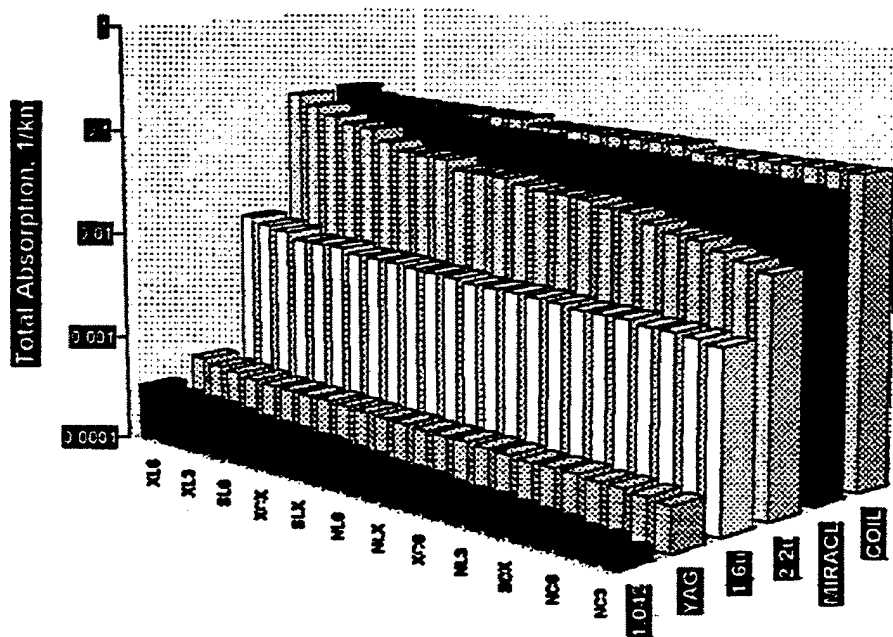**Figure 5. Atmospheric Transmittance for 0-15 μm, From Ref. [5]**

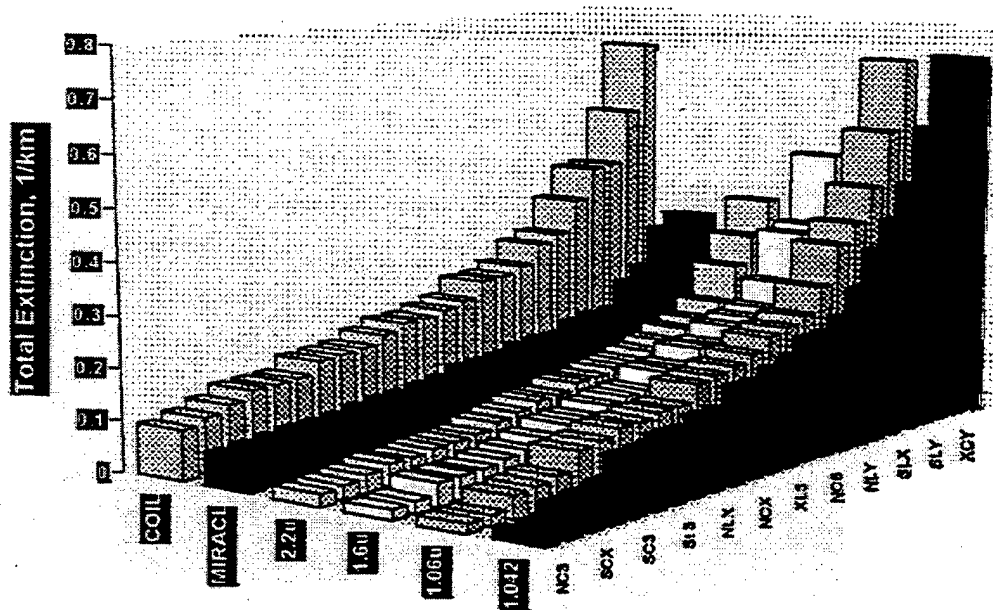**Figure 6. Total Absorption 1/km, From Ref. [6]**

Figure 7. Total Extinction 1/km From Ref. [6]

The FEL, which can be designed for a wide range of wavelengths, is the only laser capable of producing this exact wavelength. In addition to design flexibility, once the FEL is built it can be easily modified by changing the electron beam energy to operate over a range of wavelengths within a factor of two. Other lasers such as chemical lasers, gas discharge lasers, excimer lasers, and x-ray lasers are confined to a specific wavelength or wavelengths by their generation mechanism. So, an analysis of the first requirement, atmospheric propagation, shows the FEL to be a viable option for a laser weapon to defend against anti-ship missiles.

5. Size and Power

Experiments in conjunction with the MIRACL program indicate that an energy flux or power density, $\Phi \approx 10 \text{ kW/cm}^2$ is needed to destroy a missile with a dwell time of a few seconds.

13

$$\Phi = \frac{P}{A} = \frac{P}{\pi(R\theta)^2}, \tag{1}$$

where P is power, A is spot size, R is the range, and θ is the beam half angle in the far field. So for a spot size of 100 cm^2, a Megawatt-class laser is required. By integrating Φ with respect to time we can find the energy deposited at the target in a given time, or fluence, F.

$$F = \int_0^\tau \Phi dt = \Phi\tau, \tag{2}$$

where τ is the pulse length and Φ is assumed constant over the pulse. By substituting Eq. (1) for Φ and the diffraction limited $\theta = 1.22 \ \lambda/D$ into Eq. (2) we get an expression for the fluence.

$$F = 0.21\frac{PD^2\tau}{(\lambda R)^2}, \tag{3}$$

where λ is the wavelength and D is the diameter of the aperture. Because of atmospheric extinction more energy is necessary at the ship to obtain the required energy at the target [Ref. 7].

$$F = 2.1x10^4 \frac{PD^2\tau}{(\lambda R)^2} T, \tag{4}$$

where $T = e^{-\alpha R}$ is the atmospheric transmittance, and α is the extinction coefficient, F [kJ/cm^2], P [MW], D [m], τ [sec], λ[μm], and R [km].

II. FEL THEORY

A.   BASIC OPERATION

A free electron laser (FEL) takes advantage of a simple physical characteristic. When bunched electrons are accelerated they emit photons coherently. A static magnetic field, transverse to the direction of a beam of relativistic electrons, causes the electrons to change directions or "wiggle," from side to side. As the bunched electrons wiggle they give off coherent radiation with proper design of the electron beam, the optical cavity, and the magnetic field. The major components of an FEL are a source of relativistic electrons, an undulator and appropriate optics for a resonant cavity [Ref. 8].

1.   Electron Beam

Electrons are produced by an electron gun, then accelerated to relativistic energies. The electron energy is, $E = \gamma mc^2$, where γ is the Lorentz factor, m is the electron mass, and c is the speed of light. Electron energies may be from a few MeV to a few GeV depending on the desired laser wavelength. Bunching of the electrons is required for optical gain to occur. The size of the accelerator is a concern for shipboard application of the FEL and electron beam quality is also important. Electron beam quality is a measure of the spread in energies of electrons throughout the beam, and is best described (smaller is higher quality) by the ratio of the spread of the Lorentz factors to the average Lorentz factor, $\Delta\gamma / \gamma$. A typical layout for an FEL with a recirculating electron beam is shown in Figure (8).
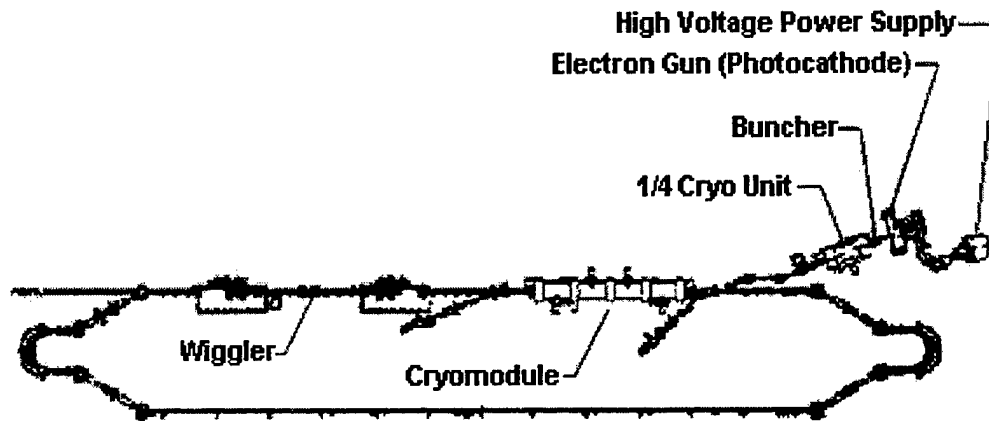
Figure 8. FEL Electron Source

2. Undulator

In the undulator, the optical field is formed and amplified by the interaction of the relativistic electron beam with the spatially periodic magnetic field. The magnetic field is produced by the alternating polarity arrangement of the magnets. A picture of an undulator, sometimes referred to as a "wiggler," is provided in Figure (9). The undulator wavelength, λ_0, is the distance along the beam axis between magnet pairs, and is given by, $\lambda_0 = L/N$, where L is the total length of the undulator and N is the number of undulator periods. The magnetic field can be produced by electromagnets, but most FEL undulators are generally constructed with permanent magnets as in Figure (9).
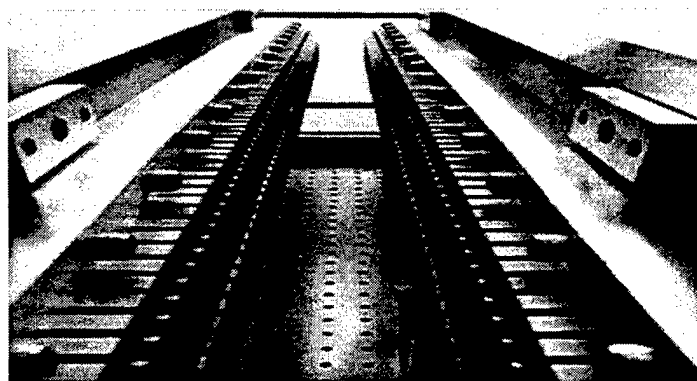

Figure 9. FEL Undulator

3. Optical Cavity

The optical cavity is oriented along the undulator axis and extends beyond the undulator length. In Figure (10), the arrows in the center represent the undulator periods, which are bracketed by mirrors containing the optical field. During successive passes through the undulator, the optical field is amplified and some fraction of the coherent radiation is allowed to escape and used in the weapon system. The physics of the FEL can be described by two equations – one for the electron motion and one for the optical field evolution. These equations will be described in detail in the following section.

FREE ELECTRON LASER RESEARCH
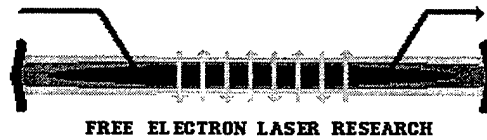
Figure 10. FEL Optical Cavity

B. PENDULUM EQUATION

It will be shown that the pendulum equation describes the transfer of momentum and energy between a free electron and the electromagnetic wave in the magnetic field of the undulator. The governing force equations for the electron are the relativistic Lorentz equations,

$$\frac{\partial(\gamma\vec{\beta})}{\partial t} = -\frac{e}{mc}[\vec{E}_r + \vec{\beta} \times (\vec{B}_r + \vec{B})], \tag{5}$$

$$\frac{d\gamma}{dt} = -\frac{e}{mc}\vec{\beta} \cdot E_r, \tag{6}$$

$$\gamma^{-2} = 1 - \vec{\beta} \cdot \vec{\beta}, \tag{7}$$

17

where $\bar{\beta}$ is the velocity of the electron as a fraction of the speed of light. The electrical field and magnetic field of the optical wave are given by,

$$\bar{E}_r = E_0[\cos(\Psi), \sin(\Psi), 0], \tag{8}$$

$$\bar{B}_r = B_0[\sin(\Psi), \cos(\Psi), 0], \tag{9}$$

where $\Psi = kz - \omega t + \phi$, the wave number is $k = 2\pi/\lambda$, ω is the angular frequency, ϕ is the optical phase angle, and λ is the optical wavelength. The undulator static magnetic field is represented by,

$$\bar{B} = B_0[\cos(k_0 z), \sin(k_0 z), 0], \tag{10}$$

where the undulator wave number is $k_0 = 2\pi/\lambda_0$, and λ_0 is the undulator wavelength. Substituting the fields in Eq. (8), (9), and (10) into Eq. (5), and resolving the transverse components gives,

$$\frac{\partial(\gamma\bar{\beta}_\perp)}{\partial t} = -\frac{e}{mc}[E_0(1-\beta_z)(\cos(\Psi), -\sin(\Psi), 0) + B_0\beta_z(-\sin(k_0 z), \cos(k_0 z), 0)], \tag{11}$$

where $\bar{\beta}_\perp$ is the transverse electron velocity and β_z is the electron velocity in the direction of the undulator axis. For a relativistic electron $E_0(1-\beta_z) \approx E_0/2\gamma^2$, which can be neglected for $\gamma \gg 1$, leaving,

$$\frac{\partial(\gamma\bar{\beta}_\perp)}{\partial t} = -\frac{e}{mc}B_0\beta_z[-\sin(k_0 z), \cos(k_0 z), 0]. \tag{12}$$

Eq. (12) can be integrated in time with the constant of integration set to zero indicating ideal injection of electrons. The result is,

$$\bar{\beta}_\perp = -\frac{K}{\gamma}[\cos(k_0 z), \sin(k_0 z), 0], \tag{13}$$

18

where we have defined an undulator parameter $K = eB_0\lambda_0 / 2\pi mc^2$. The undulator parameter allows adjustment of the transverse electron velocity by adjusting the undulator magnetic field intensity or the spacing between magnets.

Insert Eq. (8) and Eq. (13) into Eq. (6) to get,

$$\dot{\gamma} = \frac{d\gamma}{dt} = -\frac{eE_0 K}{\gamma mc^2}\cos(\zeta + \phi), \tag{14}$$

$$\frac{\dot{\gamma}}{\gamma} = -\frac{eE_0 K}{\gamma^2 mc^2}\cos(\zeta + \phi), \tag{15}$$

where the electron phase is $\zeta = (k + k_0)z - \omega t$. The initial phase at time $t = 0$ is $\zeta_0 = (k + k_0)z_0$, but since $k \gg k_0$ we can approximate $\zeta_0 \approx kz_0 = 2\pi z_0 / \lambda$, which gives a relation between the electron phase and the optical wavelength. Insert Eq. (13) for $\vec{\beta}_\perp$ into Eq. (7) to get

$$\gamma^{-2} = 1 - \vec{\beta} \cdot \vec{\beta} = 1 - \beta_\perp^2 - \beta_z^2 = \frac{1 - \beta_z^2}{1 + K^2}. \tag{16}$$

Differentiate both sides with respect to time to get,

$$\frac{\dot{\gamma}}{\gamma} = \frac{\gamma^2 \beta_z \dot{\beta}_z}{1 + K^2}, \tag{17}$$

then using Eq.(15) substitute $\dot{\beta}_z = \ddot{\zeta}/(k + k_0)c$, and solve for $\ddot{\zeta}$,

$$\ddot{\zeta} = \frac{1 + K^2}{\gamma^2}\frac{(k + k_0)c}{\beta_z}\frac{eE_0 K}{\gamma^2 mc}\cos(\zeta + \phi). \tag{18}$$

Applying approximations based on $k \gg k_0$, $\beta_z \approx 1$ when $\gamma \gg 1$, and defining dimensionless time $\tau = ct/L$, we have the pendulum equation,

$$\ddot{\zeta} = |a|\cos(\zeta + \phi), \tag{19}$$

19

$$|a| = \frac{4\pi NeKLE_0}{\gamma^2 mc^2},\qquad(20)$$

where $|a|$ is the dimensionless optical field, N is the number of undulator periods, L is the total length of the undulator, and $(\dot{\_}) = d(\_)/d\tau$.

C. OPTICAL WAVE EQUATION

The second part of the mathematical description of an FEL is the wave equation. Beginning with Maxwell's wave equation for the vector potential $\vec{A}$ such that

$$\vec{E}_r = -\frac{1}{c}\frac{\partial \vec{A}}{\partial t},\qquad(21)$$

$$\vec{B}_r = \vec{\nabla} \times \vec{A},\qquad(22)$$

$$\left[\vec{\nabla}^2 - \frac{1}{c^2}\frac{\partial^2}{\partial t^2}\right]\vec{A} = -\frac{4\pi}{c}\vec{J}_\perp,\qquad(23)$$

where $\vec{J}_\perp$ is the transverse current density and

$$\vec{A}(z,t) = \frac{c}{\omega}E(z,t)[\cos(\Psi), -\sin(\Psi), 0],\qquad(24)$$

where the optical phase is $\Psi = kz - \omega t + \phi(z,t)$. Taking two spatial derivatives and two time derivatives of Eq. (24) yields,

$$\frac{\partial^2 \vec{A}}{\partial z^2} = \frac{1}{k}\frac{\partial E}{\partial z}\left[k + \frac{\partial \phi}{\partial z}\right][\cos(\Psi), -\sin(\Psi), 0]$$

$$+\frac{1}{k}\frac{\partial^2 E}{\partial z^2}[\sin(\Psi), \cos(\Psi), 0] + \frac{1}{k}\frac{\partial E}{\partial z}\left[k + \frac{\partial \phi}{\partial z}\right][\cos(\Psi), -\sin(\Psi), 0]$$

$$+\frac{E}{k}\frac{\partial^2 \phi}{\partial z^2}[\cos(\Psi), -\sin(\Psi), 0] + \frac{E}{k}\left[k + \frac{\partial \phi}{\partial z}\right]^2[-\sin(\Psi), -\cos(\Psi), 0],\qquad(25)$$

and

$$\frac{\omega}{c}\frac{\partial^2 \vec{A}}{\partial t^2} = \frac{\partial E}{\partial t}\left[\frac{\partial \phi}{\partial t} - \omega\right][\cos(\Psi), -\sin(\Psi), 0] + \frac{\partial^2 E}{\partial t^2}[\sin(\Psi), \cos(\Psi), 0]$$

$$+ \frac{\partial E}{\partial t}\left[\frac{\partial \phi}{\partial t} - \omega\right][\cos(\Psi), -\sin(\Psi), 0] + E\frac{\partial \phi^2}{\partial t^2}[\cos(\Psi), -\sin(\Psi), 0]$$

$$+ E\left[\frac{\partial \phi}{\partial t} - \omega\right]^2[-\sin(\Psi), -\cos(\Psi), 0]. \tag{26}$$

Next, assume the optical phases and amplitudes are slowly varying in time and space such that $\partial E/\partial z \ll kE$, $\partial\phi/\partial z \ll k\phi$, $\partial E/\partial t \ll \omega E$, $\partial\phi/\partial t \ll \omega\phi$, and $\omega = kc$. Eliminate second-order terms and insert Eq. (25) and Eq. (26) into Eq. (23) to get

$$\left[\vec{\nabla}^2 - \frac{1}{c^2}\frac{\partial^2}{\partial t^2}\right]\vec{A} \approx 2\left[\frac{\partial E}{\partial z} + \frac{1}{c}\frac{\partial E}{\partial t}\right][\cos(\Psi), \sin(\Psi), 0]$$

$$+ 2E\left[\frac{\partial \phi}{\partial z} + \frac{1}{c}\frac{\partial \phi}{\partial t}\right][-\sin(\Psi), -\cos(\Psi), 0] \approx -\frac{4\pi}{c}\vec{J}_\perp. \tag{27}$$

The current density for a single electron is $\vec{J}_\perp = -ec\vec{\beta}_\perp$. Substituting Eq. (13) for $\vec{\beta}_\perp$, and introducing new time and space coordinates, $\tau = ct/L$, and $\tilde{z} = z - ct$, we have,

$$2\left[\frac{1}{L}\frac{\partial E}{\partial \tau}\right][\cos(\Psi), \sin(\Psi), 0] + 2E\left[\frac{1}{L}\frac{\partial \phi}{\partial \tau}\right][-\sin(\Psi), -\cos(\Psi), 0] \approx$$

$$-\frac{4\pi eK}{\gamma}[\cos(k_0\tilde{z}), \sin(k_0\tilde{z})]. \tag{28}$$

The dimensionless time τ progresses from zero to one from the beginning of the undulator to the end, and the coordinate $\tilde{z}$ follows a point on the optical pulse traveling at speed c. Insert Eq. (28) into Eq. (27), take the average $\langle...\rangle$ over many sample

21

electrons, and multiply by the electron particle density, ρ, giving the equations of motion for the optical field amplitude and phase,

$$\frac{\partial E}{\partial \tau} = -\frac{2\pi e \rho L K}{\gamma}\langle\cos(\zeta + \phi)\rangle, \tag{29}$$

$$\frac{\partial \phi}{\partial \tau} = \frac{2\pi e \rho L K}{\gamma}\langle\sin(\zeta + \phi)\rangle, \tag{30}$$

where $\zeta = (k + k_0)\tilde{z} - \omega t$ is the electron phase. Use the complex electric field $E = E_0 e^{i\phi}$, to get

$$\frac{\partial E}{\partial \tau} = -\frac{2\pi e \rho L K}{\gamma}\left[\langle\cos(\zeta + \phi)\rangle - i\langle\sin(\zeta + \phi)\rangle\right]e^{i\phi} = -\frac{2\pi e \rho L K}{\gamma}\langle e^{i\zeta}\rangle. \tag{31}$$

Substituting the definition of the dimensionless optical field $a = |a|e^{i\phi}$ from Eq. (13) we get the final form of the wave equation

$$\frac{\partial a}{\partial \tau} = \overset{\circ}{a} = -j\langle e^{-i\zeta}\rangle, \tag{32}$$

where the dimensionless current is $j = 8\pi^2 e^2 \rho N K^2 L^2 / \gamma^3 m c^2$. The growth of the optical field, and therefore the development of laser energy, is dependent on the dimensionless current and the average electron phase. So we need both a current j and electron bunching $\langle e^{-i\zeta}\rangle \neq 0$ to produce laser energy.

III. FEL DESIGN AND PARAMETERS

A.   TJNAF FEL

The most powerful FEL ever operated is at the Thomas Jefferson National
Accelerator Facility (TJNAF). In April 1999, the laser operated continuously at 710
Watts of average power for six hours. The FEL is designed to achieve 1 kW and will
probably soon do so. Near term modifications now in the planning stage will boost the
power to 20 kW. Table (1) shows the parameters of the TJNAF FEL and compares them
to the requirements for a shipboard anti-missile defense weapon [Ref. 9].

Parameter	TJNAF FEL	Weapon FEL
Average Power	$\bar{P} = 1$ KW	$\bar{P} = 1$ MW
Average Current	$\bar{I} = 5$ mA	$\bar{I} = 900$ mA
Electron Energy	$\gamma mc^2 = 48$ MeV	$\gamma mc^2 = 100$ MeV
Lorentz Factor	$\gamma = 94$	$\gamma = 196$
Undulator Field	$B_0 = .38$ T	$B_0 = .27$ T
Undulator Wavelength	$\lambda_0 = 2.7$ cm	$\lambda_0 = 4$ cm
Undulator Periods	$N = 40$	$N = 25$
Undulator Length	$L = 108$ cm	$L = 100$ cm
Undulator Parameter	$K = 0.96$	$K = 1$
Rayleigh Length	$z_0 = 40$ cm	$z_0 = 10$ cm
Electron Charge/Bunch	$I_e/c = 60$ pC	$I_e/c = 1800$ pC
Peak Current	$\hat{I} = 60$ A	$\hat{I} = 600$ A
Electron Beam Radius	$r_b = 100$ μm	$r_b = 300$ μm
Pulse Length	$\tau = 0.4$ ps	$\tau = 3$ ps
Pulse Repetition Rate	$PRR = 18.7/37.4/74.85$ MHz	$PRR = 500$ MHz
Optical Resonator Length	$L_{opt} = 8.01$ m	$L_{opt} = 10$ m
Output Coupling	10%	10%
Resonator Cavity Losses	$Q = <0.5\%$ / pass	$Q = <0.5\%$ / pass
Optical Wavelength	$\lambda = 3\text{-}6$ μm	$\lambda = 1$ μm

Table 1. Comparison of TJNAF FEL with a weapon FEL

The big differences are increases in the (i) peak current by a factor of 10, (ii) the repetition rate by a factor of 7, (iii) the electron beam energy by a factor of 2, and (iv) the pulse length by a factor of 7.

B.   MODELING A MW FEL

As we can see from Table (1) there is still a long way to go from the current FEL to a weapons application FEL. Since we do not have a MW-class FEL to perform experiments, we must turn to scaling to determine the effectiveness of a FEL weapon without spending hundreds of millions of dollars. As mentioned in Chapter I, power density $\Phi \approx 10$ kW/cm^2 over a spot size A ≈ 100 cm^2 is required to destroy a missile with a dwell time of a few seconds. By scaling we can get an appropriate spot size for any laser power. With a power density of $\Phi = 10$ kW/cm^2, a 100 W laser must use a spot size of 1 mm^2, and a 1 kW laser must use a spot size of 10 mm^2.

Scaling will only work, however, if the heat diffusion is independent of spot size. Schriempf gives a detailed treatment of diffusion, but a summary is useful. The heat flow equation is

$$\rho C \frac{\partial T}{\partial t} = K \nabla^2 T + A \tag{33}$$

where ρ is the material density, C is the specific heat, T temperature, t time, K thermal conductivity and A is the heat produced per unit volume per unit time [Ref. 10]. For a semi-infinite solid with no phase change and material properties that are temperature-independent, Eq. (33) reduces to

$$\frac{\partial^2 T}{\partial z^2} - \frac{1}{\kappa} \frac{\partial T}{\partial t} = -\frac{A}{K}, \tag{34}$$

where the thermal diffusivity is $\kappa = K/\rho C$. The heat produced per unit volume per unit time is given by

$$A(z,t) = (1 - \Re)\Phi(t)\alpha e^{-\alpha z},\qquad(35)$$

where $\Re$ is the reflectivity, $\Phi(t)$ is the power density at depth z, and α is the absorption coefficient. At optical wavelengths, for most solid materials, the absorption coefficient is very large $\alpha \approx 10^6$/cm. The exponential term approaches zero, and A is small compared to the time and space derivative terms. As a result we can assume $A \approx 0$ and Eq. (35) becomes

$$\frac{\partial^2 T}{\partial z^2} - \frac{1}{\kappa}\frac{\partial T}{\partial t} = 0.\qquad(36)$$

The solution to Eq. (36) is

$$T(z,t) = \frac{\Phi_0 D}{K}\, ierf\left[\frac{z}{D}\right],\qquad(37)$$

where Φ_0 is the constant power density on the target and the characteristic thermal diffusion length is $D = 2\sqrt{\kappa t}$ which represents the distance required for T to drop to $1/e$ times its initial value. In the semi-infinite approximation we ignored radial heat flow, but in order for this to be valid the spot size must be much larger than D, or the target diameter $d \leq D$. If these conditions are not met, we expect heat to diffuse outside of the laser spot and the spot will not be heated effectively.

One of the targets to be irradiated was Al-6061. A calculation of the thermal diffusion length associated with heating the sample to melting temperature was performed with $\rho = 2700$ Kg/m^3, $C = 896$ J/Kg-K, K = 180 W/m-K, $\kappa = 7.44 \times 10^{-5}$ m^2/s, $T_m = 855$K, $\Phi_0 = 10^8$ W/m^2 and

$$D = 2\sqrt{\kappa\tau}, \qquad (38)$$

$$\tau = \frac{\pi K^2 \Delta T^2}{4\Phi_0^2 \kappa}, \qquad (39)$$

Where τ is the time required to bring the material from ambient temperature to melting temperature and ΔT is the temperature change. The result for Al-6061 was $D = 1.79$ mm. In order to melt through an aluminum sample, the scaled laser spot must have an area $A \gg \pi(1.79 \text{ mm})^2 = 10 \text{ mm}^2$ or the target itself made small with $d \approx D$. These calculations were experimentally verified with samples of Al-6061. Using $d = 1$ cm, the sample was irradiated with no melting after several minutes. Other samples with $d = 2$ mm were melted in a few seconds.

Another target to be irradiated was Slip-cast Fused Silica (SiO_2). A calculation of the thermal diffusion length associated with heating the sample to its melting temperature was performed with $\rho = 2200 \text{ Kg/m}^3$, $C = 920 \text{ J/Kg-K}$, $K = 1.26 \text{ W/m-K}$, $\kappa = 5 \times 10^{-7}$ m^2/s, $T_m = 1980K$ [Ref. 11], $\Phi_0 = 10^8 \text{ W/m}^2$ and the result was $D = 0.021$ mm. Therefore, with the insulating material, fused silica, the scaled laser spot must have an area $A \gg \pi(0.021 \text{ mm})^2 = 0.0014 \text{ mm}^2$, which is attained with the 1 mm^2 beam used at TJNAF.

C. PULSE TRAIN

Since there is growing interest in lasers for many scientific and engineering applications, research into short pulse effects has increased sharply in the last few years. The pulse train of an FEL is different from any other laser and its interaction with matter

at high-average power has not been studied. The TJNAF FEL has a pulse length of

$\tau = 0.4$ ps and a repetition period of $T = 27$ ns illustrated in Figure (11). The duty cycle

D is the fraction of time the laser is actually irradiating the target,

$$D = \frac{\tau}{T} = \frac{4 \times 10^{-13} s}{2.7 \times 10^{-8} s} = 1.5 \times 10^{-5}.$$ (40)

The peak power in each micropulse $\hat{P}$ is

$$\hat{P} = \frac{\overline{P}}{D} = \frac{710W}{1.5 \times 10^{-5}} = 47MW,$$ (41)

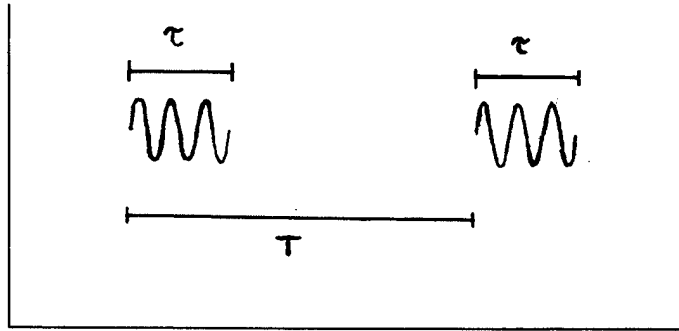Where $\overline{P}$ is the average power of 710 W.

Figure 11. FEL Pulse Format

Comparing the TJNAF FEL to another short pulse laser is instructive. The

Lawrence Livermore National Labs (LLNL) 1.053-μm Ti:sapphire CPA system [Ref. 12]

has a pulse length $\tau = 0.4$ ps, but a pulse repetition rate of only 10 Hz, so the period is

$T = 0.1$ s, and the peak power is $\hat{P} = 2.5TW$. The duty factor is

$$D = \frac{4 \times 10^{-13} s}{0.1s} = 4 \times 10^{-12},$$ (42)

so that the average power is

27

$$\overline{P} = \left(2.5 \times 10^{12}\,W\right)\left(4 \times 10^{-12}\right) = 10W \,. \tag{43}$$

Note that the LLNL laser has a much higher peak power than the TJNAF FEL, but the TJNAF FEL has more than seventy times the average power because of its high duty cycle. The experiments detailed in the following section were conducted to study the effects of the unique FEL pulse format in laser-matter interaction on small samples.

IV. FEL EXPERIMENTS

A. LABORATORY LAYOUT

Experiments for this thesis were conducted at the Thomas Jefferson National Accelerator Facility (TJNAF), which is operated by the Southeastern Universities Research Association (SURA) for the U. S. Department of Energy (DOE). Once a laser beam has been created, as described in chapter two, the beam is sent by a low-loss optical path to user laboratories in another part of the building. User laboratory number one was used for all experiments described below. M. Shinn, S. Benson, B. Yunn, G. Neil, K. Jordan and J. Gubeli operated the laser and other laboratory equipment. The optical bench was configured with a focusing lens, a sample holder and two video cameras. One camera was focused on the front of the sample and one on the back of the sample as shown in Figures (12) and (13).
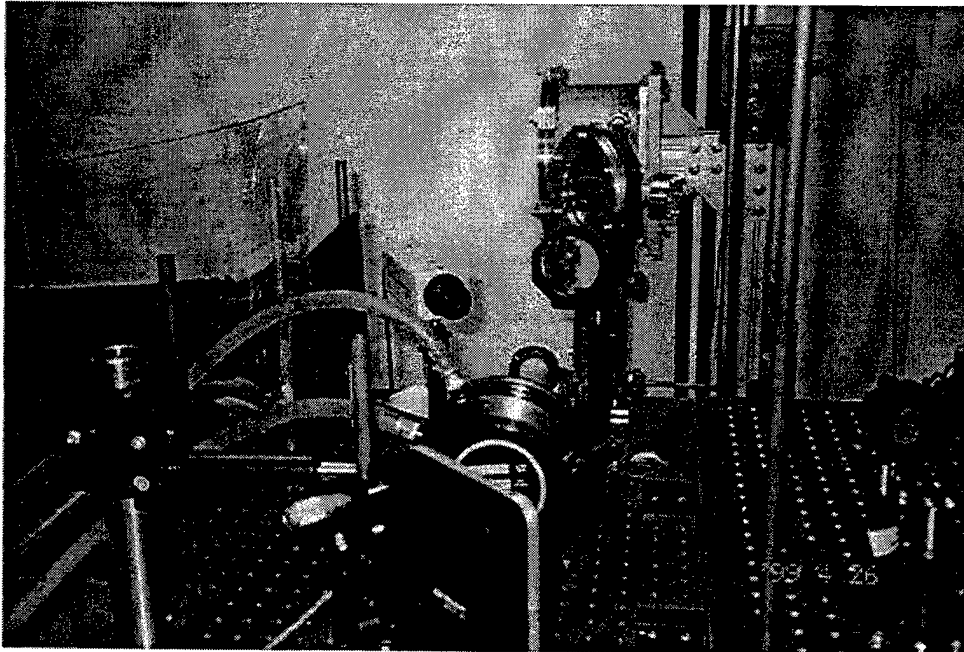

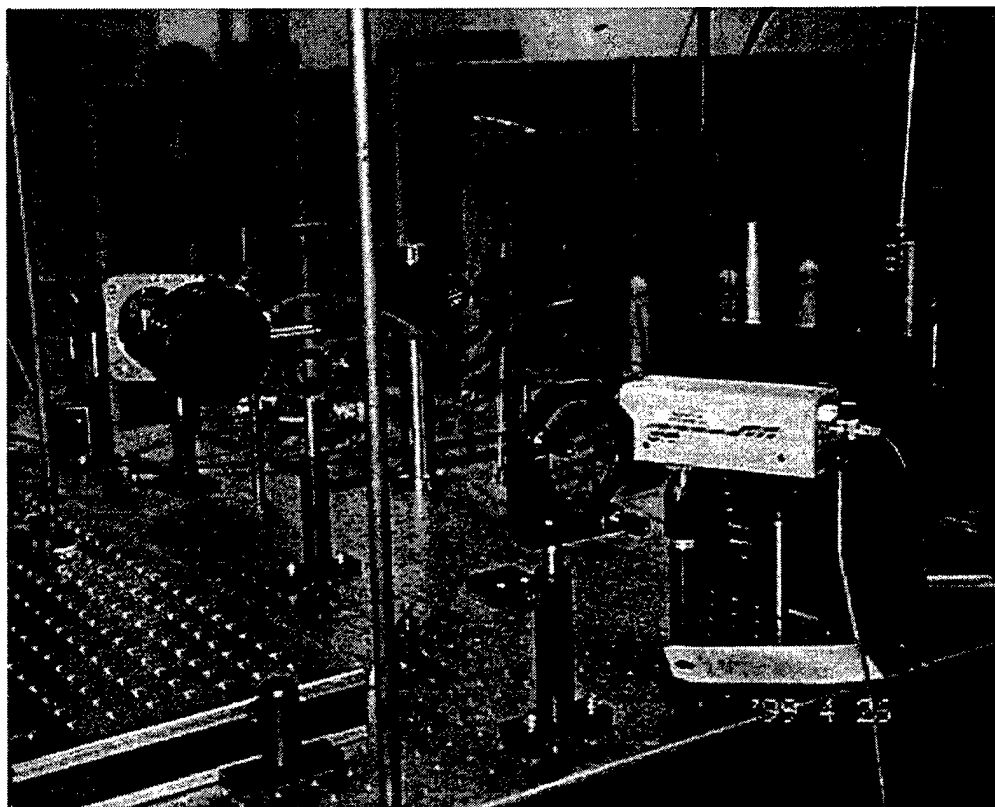**Figure 12. Back view of sample in user lab arrangement**

Figure 13 Front view of sample in user lab arrangement

B.   EXPERIMENTAL PROCEDURE

Samples were irradiated by a laser beam with wavelength $\lambda = 4.825$ μm through a calcium fluoride lens with a focal length of 300 mm. The pulse repetition frequency (PRF) was 37.425 MHz and the average power meter in the user lab read 100-103 W with an error of +/- 5 W. Since a lens focused the beam, the beam area decreased with distance along the direction of propagation to a minimum waist radius of $w_0 = 80$ μm at the focal point. Paraxia, a beam propagation code, was used to model the beam diffraction and find the target position giving the desired intensity of 10 kW/cm^2 [Ref. 13]. Figure (14) shows a graph of irradiance versus distance from the focal point, with the negative numbers indicating positions in front of the focus.
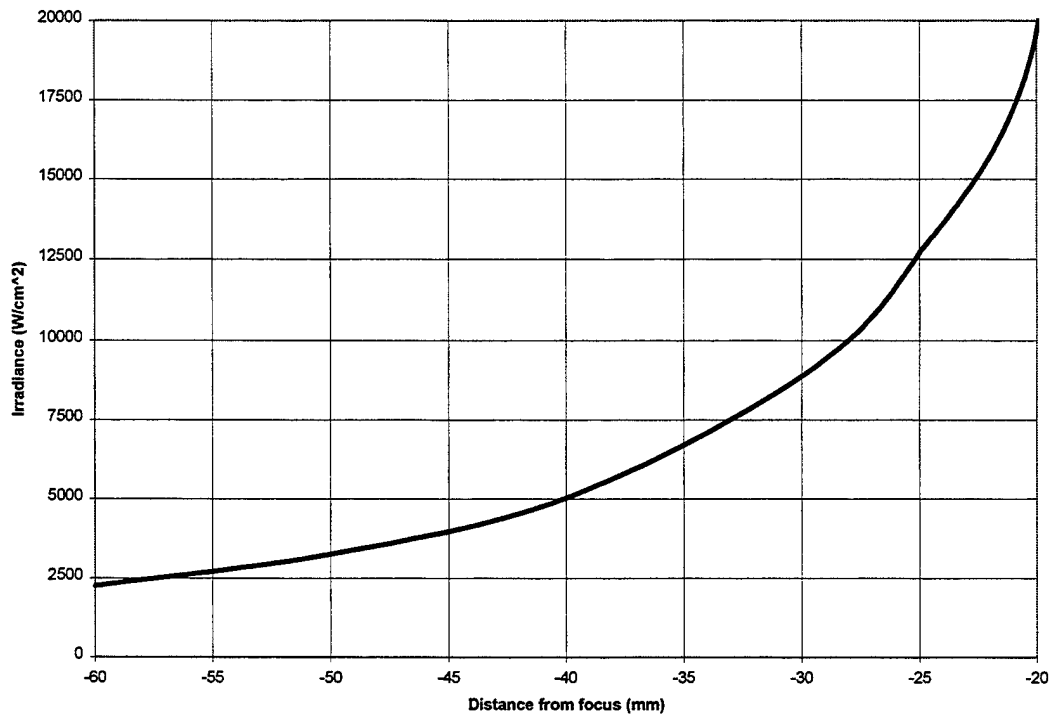
Figure 14. Irradiance vs. Distance from Focal Point, From Ref. [13]

An irradiance of 10 kW/cm^2 occurs when the sample position is between 25-30 mm in front of the focal point. The samples were actually placed 26 mm in front of the focus. The burn-through time was determined by observing a signal on a power meter placed behind the samples, and by watching for the presence of coherent harmonics in the visible spectrum on an iris placed approximately 15 cm behind the samples.

C.   DESCRIPTION OF RESULTS

The Naval Research Laboratory (NRL) provided the sample materials, which included Slip-cast Fused Silica (SiO$_2$), Polyimide Fiberglass, and F2 Epoxy. The last two were from the same batch as the material used for previous continuous wave (CW) laser penetration studies.

31

1. Sample #1 Slip-cast Fused Silica

The sample provided by NRL is 6.9 cm by 7.4 cm and varies in thickness from 0.9 cm to 1.9 cm. The front of the sample after irradiation is shown in Figure (15).
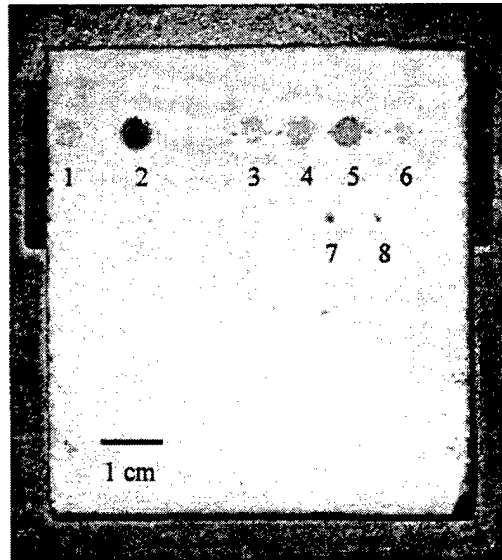

Figure 15. Slip-cast fused silica sample

The sample was irradiated eight times and the results are summarized in Table (2).

Run Number	Average Intensity (kW/cm^2)	Exposure Time (s)	Penetration Depth Rate (mm/s)
1	9	9	0.20
2	9	110	0.081
3	9	13	0.20
4	9	24	0.125
5	9	41	0.081
6	9	2	0.35
7	500	3	3.0
8	500	11	3.0

Table 2. Irradiation of Slip-cast Fused Silica, After Ref. [14]

The irradiations were done from left to right. The last two runs were done with the sample at the focus instead of 26 mm in front so that the beam waste radius was $w = w_0 = 80\ \mu m$ and the intensity was $500\ kW/cm^2$. The last two runs were conducted to investigate the effects of much higher power density. As shown in Figure (15), the first six runs were along the top of the sample and the last two were approximately 1 cm below. The second, seventh and eighth runs penetrated the entire 0.9-cm thickness of the Fused Silica material. Figure (16) shows the effects of exposure time on penetration depth rate.
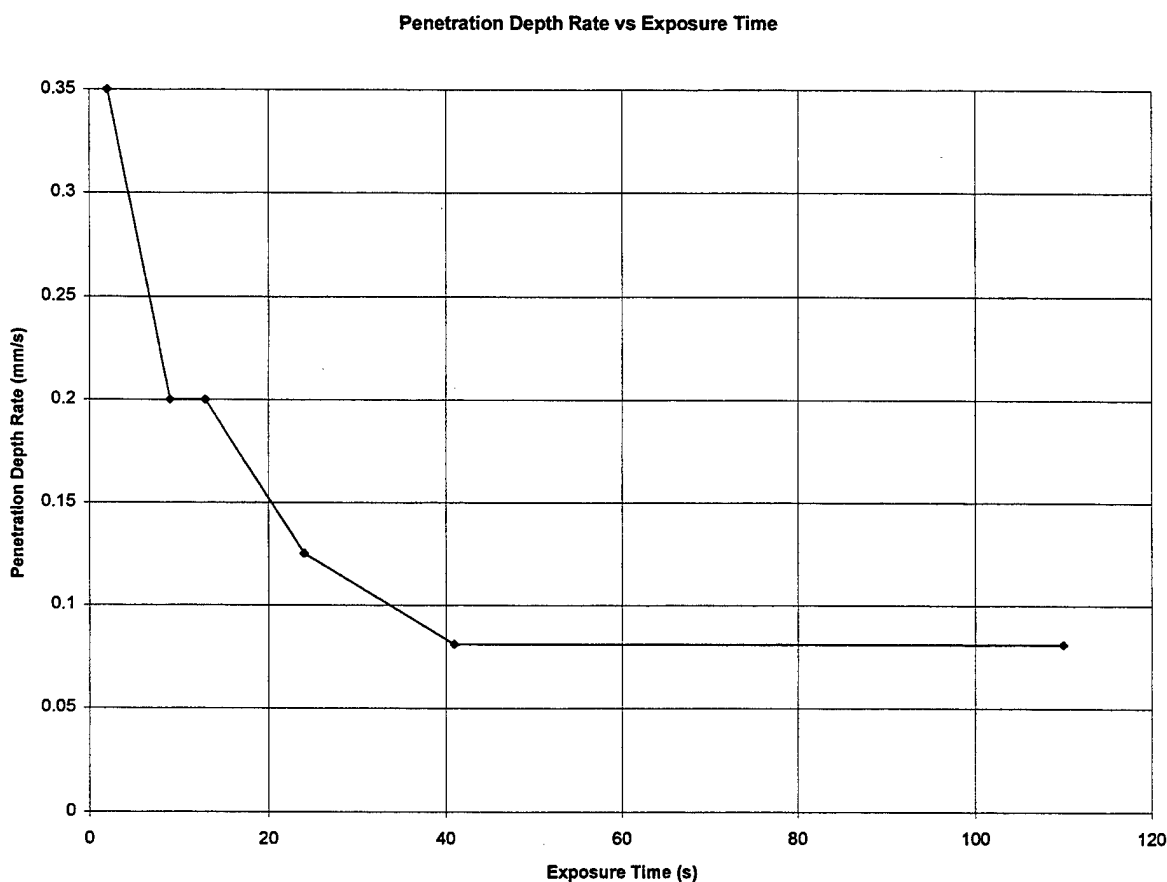
Penetration Depth Rate vs Exposure Time

Figure 16. Exposure Time vs. Penetration Depth Rate for Fused Silica

As the exposure time was increased more smoke and debris filled the hole blocking the path of the laser beam and causing the penetration depth rate to decline over time. In the future, we can explore whether altering the FEL wavelength during sample irradiation improves penetration depth rates through smoke and debris.

Since the second run was the only one to punch completely through the material that was also conducted at the primary power density of interest, we shall take a closer look at it. A digital picture of run two was taken through an optical microscope as shown in Figure (17).
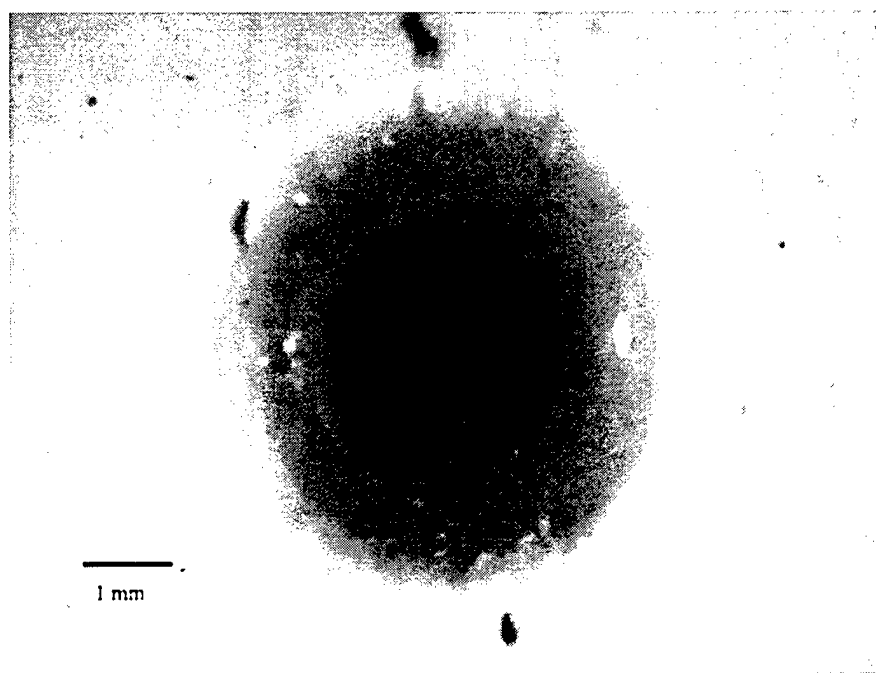

Figure 17. Close-up of damage to slip-cast fused silica in run 2

Although the beam diameter was only 1.1 mm, the melted portion at the surface of the sample measured 5 mm in diameter. The hole is tapered with the melted portion on the back of the sample measuring only 2 mm in diameter. The reasons for this are twofold.

First, the beam profile is Gaussian in nature with the highest intensity in the center of the beam and intensity down by 1/e at the beam radius. Second, the sample face is 26 mm in front of the focus and the sample back is 17mm from the focus, so the beam size is decreasing as it proceeds through the material as shown in Figure (18).
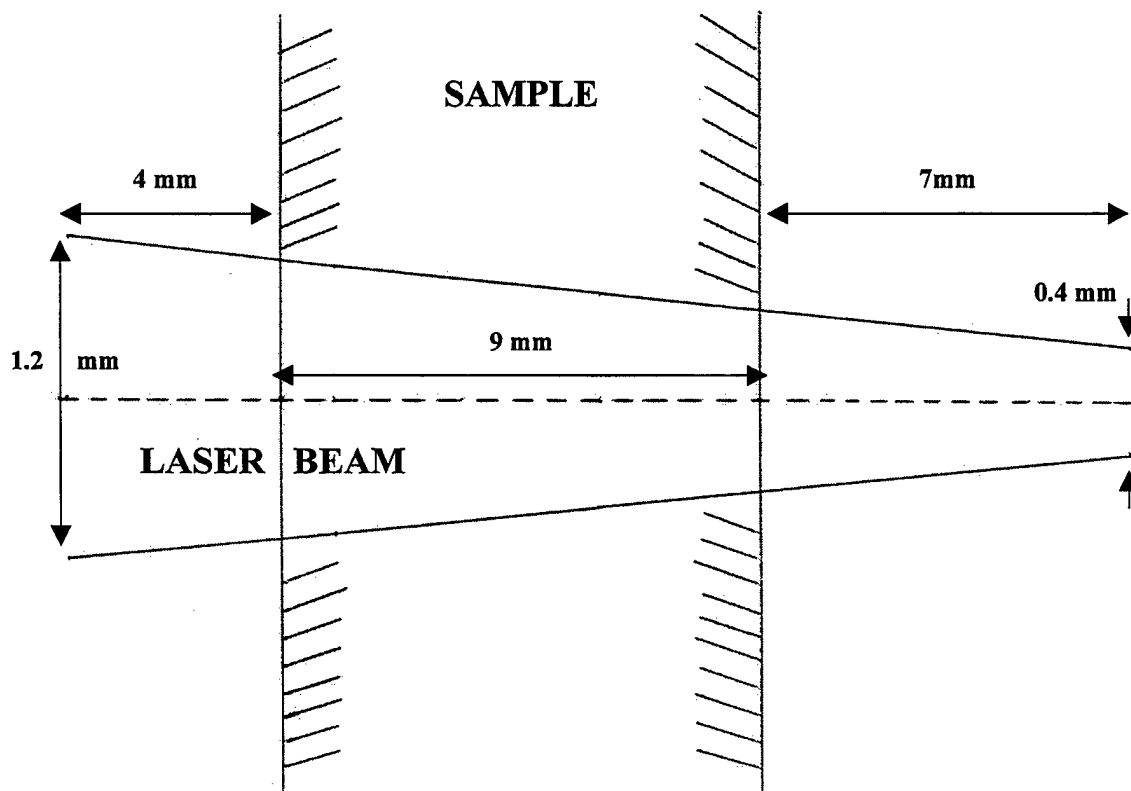
Figure 18. Sketch of beam focusing effect

The vertical scale in Figure (18) is exaggerated by a factor of five with respect to the horizontal scale in order to demonstrate the effect.

Examination of the hole from run two through an optical microscope reveals a 1-mm thick layer of melted, and rehardened, SiO_2 filling the hole at the back of the sample.

It was clear from the video and the rear power meter that burn-through occurred in run

two, but melted material solidified and sealed the hole at the back of the sample. A

picture of the back of the target taken through a Scanning Electron Microscope (SEM),

Figure (19), shows the hole from run seven is fairly irregular with a great deal of debris.
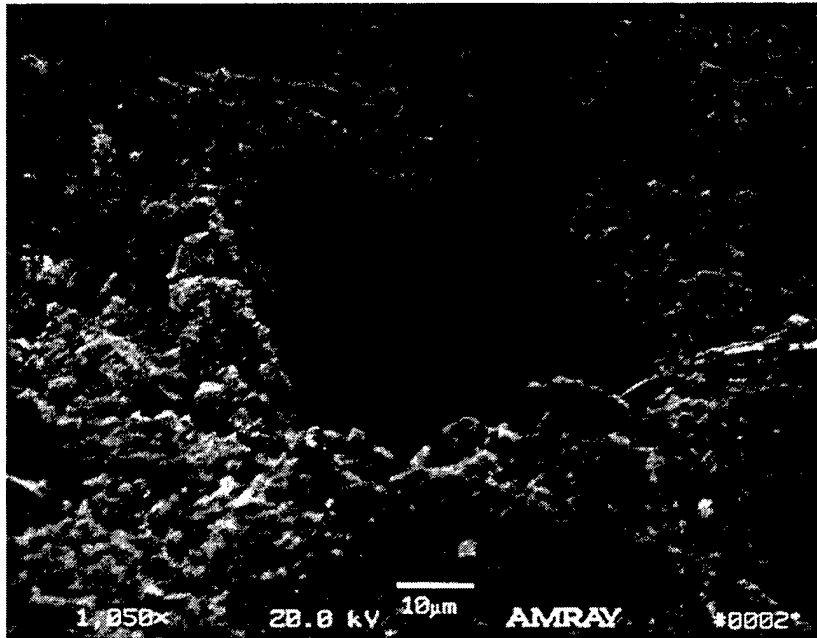

Figure 19. SEM photograph of damage to Fused Silica sample from run 7

The volume of the hole in run two is estimated by,

$$V = \int_0^{9\,mm} \pi \left[R(z) \right]^2 dz , \tag{44}$$

where the radius approximately changes linearly as

$$R(z) = 0.53mm - 0.02z , \tag{45}$$

which gives a volume of $V = 5.6$ mm^3. By a similar calculation, the volume of the entire

damaged region, including the melted and rehardened portion, is estimated to be

V = 92 mm^3. Based on the density of fused silica of ρ = 2.2 g/cm^2, the amount of material removed was 0.012 g, and the amount of material damaged was 0.20 g. The heat energy deposited during run two is given by,

$$E = P\tau = \Phi A\tau , \qquad (46)$$

which gives E = 9.7 kJ deposited during the 110 second run. The heat of ablation is then 48 kJ/g for the damaged area. In future studies this value should be correlated to the values obtained for similar materials in much larger scale CW laser experiments in the past, with appropriate compensation for experimental environment and wavelength.

2. Sample #2 Polyimide Fiberglass

The sample provided by NRL is 11.4 cm by 10.1 cm and 2 mm thick. The damaged area of the sample, after irradiation, is shown in Figure (20).
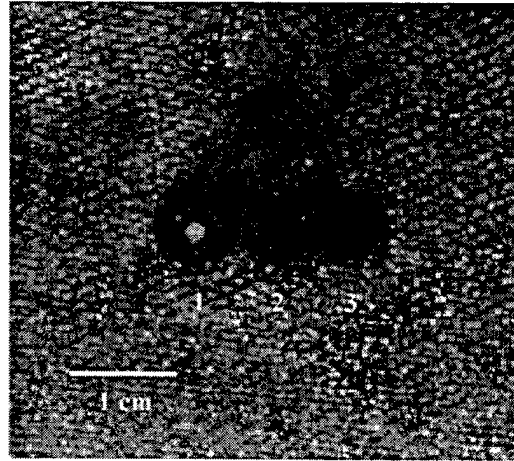

Figure 20. Polyimide Fiberglass target

The sample was irradiated three times and the results are summarized in Table (3).

Run Number	Average Intensity (kW/cm^2)	Exposure Time (s)	Penetration Depth Rate (mm/s)
1	9	7	0.28
2	9	2	0.90
3	9	1	1.1

Table 3. Irradiation of Polyimide Fiberglass, After Ref. [14]

The irradiations were done from left to right with the sample 26 mm in front of the focus of the beam. Only the first run achieved burn-through of the material, with the entry hole 3 mm in diameter and the exit hole 1.5 mm. All three holes show significant charring adds an additional term to the heat transport equation and impedes ablation. Investigation with an optical microscope reveals a raised lip of material around the face of the hole that does not appear on the fused silica sample and much more roughness as observed in Figure (21)-(23). The charred region extends to a diameter of 8.0 mm for run one, 6.5 mm for run two, and 5.4 mm for run three. The lip height is 0.3 mm for run one, 0.1 mm for run two, and 0.05 mm for run three. These measurements indicate that as the dwell time increases, the radial extent of the damage area increases, and more material is deposited around the edge of the hole. There is no evidence of melted and rehardened material present in the holes as found with the fused silica indicating a different mechanism for ablation in the two samples.
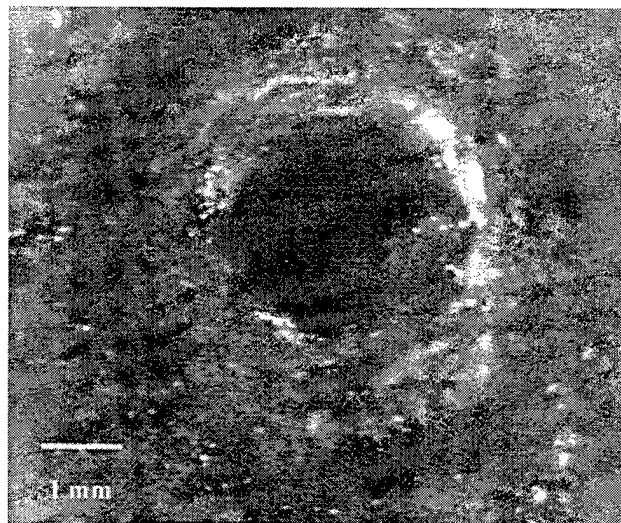
Figure 21. Close-up of damage to Polyimide fiberglass in Run 1
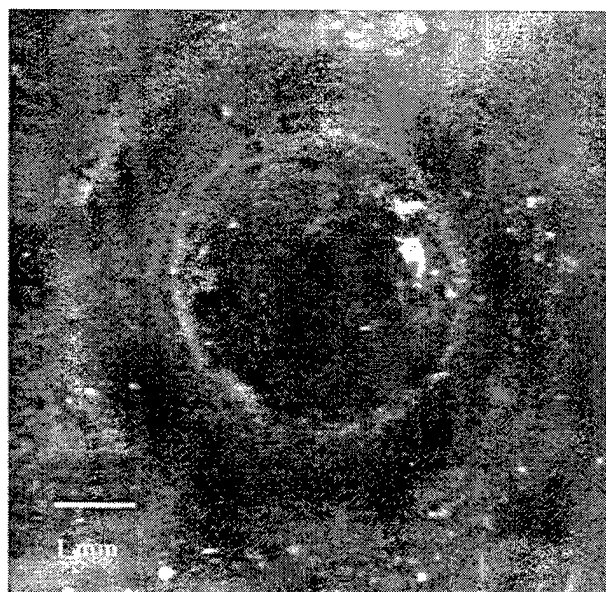
Figure 22. Close-up of damage to Polyimide fiberglass in Run 2

Figure 23. Close-up of damage to Polyimide Fiberglass in Run 3

3. Sample #3 F2 Epoxy

The sample provided by NRL is 10.0 cm by 11.5 cm and 1.5-mm thick including a 1.6-cm thick polyurethane foam backing. The damaged area of the sample, after irradiation, is shown in Figure (22).

Figure 24. F2 Epoxy sample

The sample was irradiated three times and the results are summarized in Table (4).

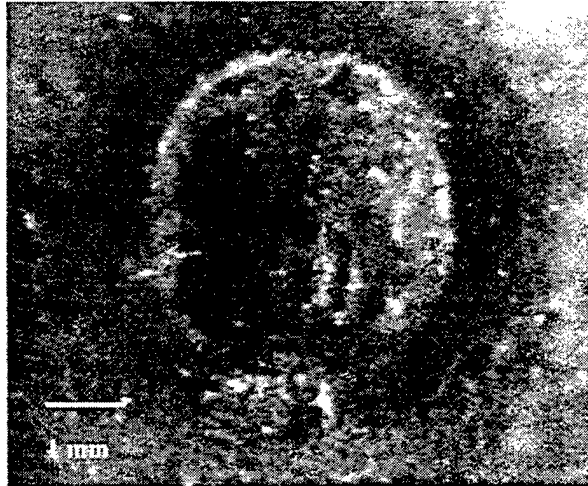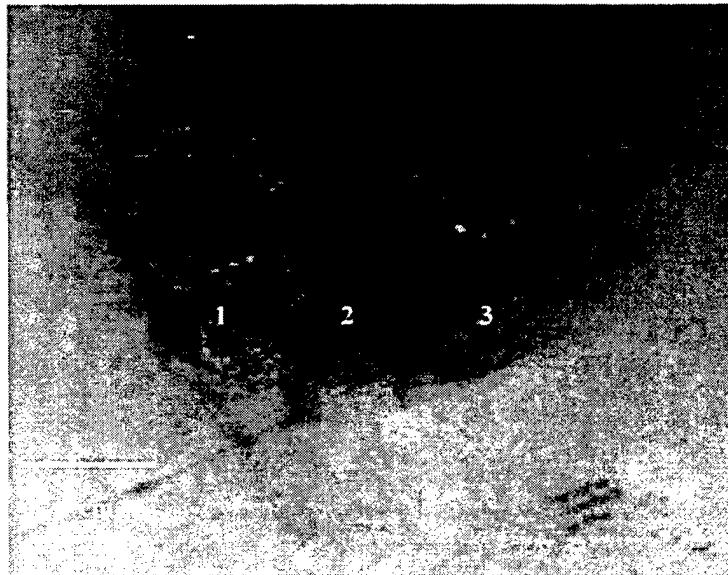| Run Number	Average Intensity (kW/cm^2)	Exposure Time (s)	Penetration Depth Rate (mm/s)
1	9	11	0.10
2	9	6	0.12
3	9	3	0.10

Table 4. Irradiation of F2 Epoxy, After Ref. [14]

In each case, it appears that the F2 Epoxy was completely penetrated and the ablation of the foam backing had begun, but not completed. The videotape showed flames engulfing the upper portion of the sample and Figure (24) shows the black charred area extending to the edge of the sample. Significant charring was evident when the sample was viewed with the optical microscope, very similar to the Polyimide sample. There was also evidence of some melting, but not as much as occurred in the Fused Silica sample. The holes appear to be filled with the charred debris of the polyurethane backing, making hole depth measurements difficult and rendering penetration depth rates unreliable. Figures (25)-(27) show the details of runs one through three.

Figure 25. Close-up of damage to F2 Epoxy in run 1
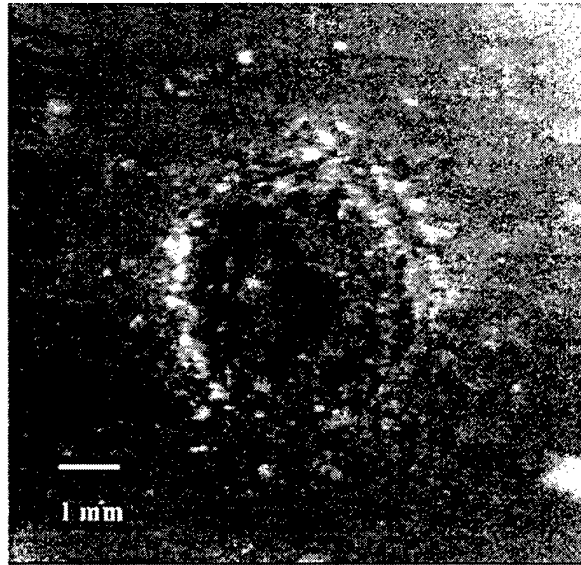
Figure 26. Close-up of damage to F2 Epoxy in run 2
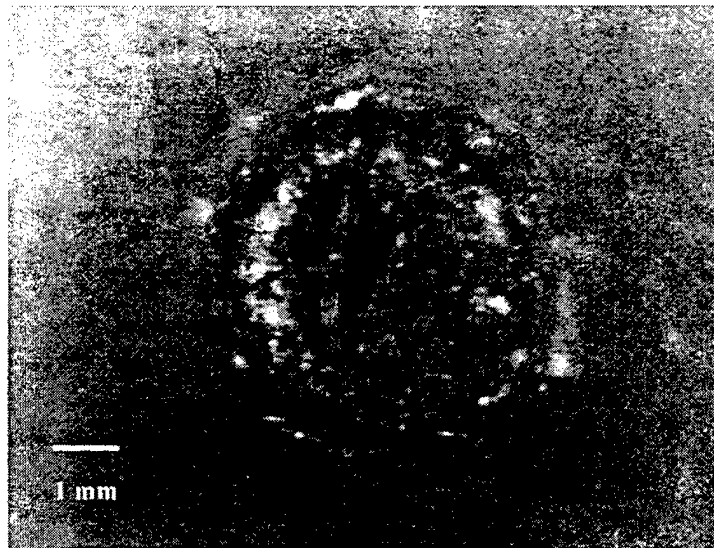
Figure 27. Close-up of damage to F2 Epoxy in run 3

The damaged region extends to a diameter of 11.3 mm for run one, 7.5 mm for run two, and 5.2 mm for run three. There is a lip around each of the holes, but much smaller than the polyimide sample showed. The lip for run one was 0.05 mm and for runs two and

three the lip was too small to measure with the optical microscope mechanism. These measurements indicate that as dwell time increases the radial extent of the damage area increases, and more material is deposited around the edge of the hole. When wind is added to the test, we may observe that debris in the hole is removed during irradiation.

V. CONCLUSIONS

In this thesis, it was established that a new self-defense weapon is needed to counter current and future threats to U. S. Navy ships. The FEL was proposed as a possible alternative to the inadequate CIWS because of its speed-of-light "bullets", unlimited magazine, tunability, and power. The basic physics of the FEL was described through the derivations of the pendulum equation and the optical wave equation. The Navy's Directed Energy Office has already selected the FEL for developmental funding, so experimentation is required to determine the direction development should take. This thesis describes the first measurements of laser damage from the newly developed TJNAF FEL and the results could provide the basis for new directions for directed energy weapons design.

A. SCALING

The TJNAF FEL, which is capable of several hundred Watts of continuous average power, was used to simulate the damage from a MW-class weapon by focusing the beam to a smaller spot size. The eventual goal is to develop scaling rules that will reliably predict the damage of a large laser without having to bare the enormous cost of building the large laser first. The experimental data shows that the scaling concept with thermal diffusion calculations is promising. More detailed experiments varying wavelength, power, and spot size may be able to produce scaling laws, which would be invaluable, for future weapons designers.

B.   FEL PULSE FORMAT

The extremely short sub-picosecond pulse length of the FEL beam is a result of the electron bunches described in the section on FEL background physics. The TJNAF FEL has a unique pulse format with a rapid sequence of short, powerful pulses. The peak power in each pulse is about 50 MW lasting for only about one-half picosecond coming at a rate of 37 MHz. Other studies have shown that such short pulses may give as much as a factor of ten advantage in reduced fluence required to produce damage [Ref. 15]. The experiments conducted for this thesis began to collect data to show whether this advantage exists, but further experimentation will be required.

C.   FUTURE EXPERIMENTS

The TJNAF FEL is scheduled for an upgrade to 20 kW of power that will allow more flexibility in scaling experiments and further tests of scaling itself. Additional plans are for experiments, which include wind passing over the samples, weighing of the samples before, and after each run, new wavelengths, changing wavelength during irradiation, new pulse formats, and other sample materials. As experimental procedures are refined and the amount of data increases, more thorough analysis of the FEL beam and comparison to other lasers will become possible.

LIST OF REFERENCES

1. Woehler, K. E., PH 4054 Course Notes, pp. 222-228, Naval Postgraduate School, 1998.

2. Benford, J. and Swegle, J., *High-Power Microwaves*, Artech House, Norwood, MA, 1991.

3. Herbert, P. A., "Anti-ship Missile Defense and the Free Electron Laser", Master's Thesis, Naval Postgraduate School, December 1998.

4. Cook, J. R. and Albertine, J. R., "High Energy Laser Weapon System", *Surface Warfare*, September/October 1997, Vol. 22, No. 5.

5. Holst, G. C., *Electro-Optical Imaging System Performance*, JCD, Winter Park, FL, 1995.

6. Cook, J. R. and Albertine, J. R., "The Navy's High Energy Laser Weapon System", SPIE, Vol. 2988.

7. Woehler, K. E., PH 4054 Course Notes, pp. 9-12, Naval Postgraduate School, 1998.

8. Colson, W. B., *Laser Handbook*, Vol. 6, Chapter 5, North-Holland, 1990.

9. Small, D. W., "Interaction of Laser Beams With Relativistic Electrons", Doctoral Dissertation, Naval Postgraduate School, March 1997.

10. Schriempf, J. T., "Response of Materials to Laser Radiation: A Short Course", Naval Research Laboratory, Washington, DC, July 1974.

11. Cozzens, R. F., "Missile Radome Materials: Vulnerability to High Energy Laser Radiation", Naval Research Laboratory, Washington, DC, June 1996.

12. Stuart, B. C., et al., "Nanosecond-to-femtosecond Laser-Induced Breakdown in Dielectrics", Physical Review Letters, Vol. 53, No. 4, January 1996.

13. Shinn, M. D., personal letter, 4 March 1999.

14. Shinn, M. D., personal letter, 13 May 1999.

15. Stuart, B. C., et al, "Optical Ablation by High-Power Short-Pulse Lasers", Journal of the Optical Society of America, 1996.

INITIAL DISTRIBUTION

1. Defense Technical Information Center 2
   8725 John J. Kingman Rd., STE 0944
   Ft. Belvoir, VA 22060-6218

2. Dudley Knox Library 2
   Naval Postgraduate School
   441 Dyer Rd.
   Monterey, CA 93943-5101

3. Engineering and Technology Curricular Office, Code 34 1
   Naval Postgraduate School
   Monterey, CA 93943

4. Professor William B. Colson, Code PH/Cw 4
   Naval Postgraduate School
   Monterey, CA 93943-5117

5. Professor Robert L. Armstead, Code PH/Ar 1
   Naval Postgraduate School
   Monterey, CA 93943-5117

6. Lieutenant Commander Robert W. Thomson Jr., USN 1
   595 D Michelson Rd.
   Monterey, CA 93940

7. John Albertine 1
   109 Kingswood Rd.
   Annapolis, MD 21401

8. Joung R. Cook 1
   Research Physicist, Code 6655
   Naval Research Laboratory
   4555 Overlook Dr., SE
   Washington, DC 20375-5000

9. Fred Dylla 1
   TJNAF
   1200 Jefferson Ave.
   Newport News, VA 23606